Holography with higher-order Stokes correlation

Tushar Sarkar,[1] Vipin Tiwari,[2] Sourav Chandra,[1] Nandan S. Bisht,[2,3] and Rakesh Kumar Singh[1,*]

[1]*Laboratory of Information Photonics and Optical Metrology, Department of Physics, Indian Institute of Technology (Banaras Hindu University), Varanasi 221005, India*

[2]*Applied Optics & Spectroscopy Laboratory, Department of Physics, Kumaun University, SSJ Campus Almora, Uttarakhand 263601, India*

[3]*Department of Physics, Soban Singh Jeena University, Almora, Uttarakhand 263601, India*

(Received 7 March 2022; accepted 30 June 2022; published 13 July 2022)

We present and experimentally demonstrate a holography technique with a higher-order Stokes correlation of the random light field. The proposed technique is capable to reconstruct the complex-valued object from the random light field, and overcome twin image issues in the higher-order correlation holography without angular shift, phase shifting, and iterations. A basic principle of the proposed technique is presented and its application is demonstrated by establishing a connection between the higher-order Stokes fluctuations correlations and the far-field complex coherence function of the random field in a lensless configuration. The viability of our technique is demonstrated by considering incoherent reconstruction of the hologram and reconstructing the complex-valued information encoded into the hologram as a distribution of complex coherence function.

DOI: 10.1103/PhysRevA.106.013508

I. INTRODUCTION

Holography relies on the principle of interference between the coherent waves. A complex field of the wave is preserved in an optically recorded interference pattern known as a hologram [1–4]. A digitally recorded hologram is used to coherently reconstruct the three-dimensional (3D) information using numerical propagation and the technique is referred to as digital holography (DH) [4,5]. The DH offers a fast recording and reconstruction process which has opened new avenues for nondestructive testing, medical diagnosis, 3D display technologies, and quantitative imaging, to name a few [4,6–8]. Various DH schemes with different geometries have been developed in the past and vital among them are in-line, off-axis, phase-shifting, and Fourier transform holography (FTH) [1–5]. The holography with an off-axis geometry requires an angular separation between the interfering beams to eliminate the twin image of the in-line holography. To circumvent a twin image issue, different experimental schemes have been proposed and significant among them are off-axis, and phase-shifting holography [2,3]. Off-axis holography requires a carrier frequency while recording the hologram to avoid the overlapping of the image with the conjugate image alias [2,9]. However, an off-axis holography geometry affects the reconstruction quality due to limited pixel size in the image sensors and sharing of the frequency space [8]. Phase-shifting holography overcomes this issue by capturing several images with accurate different phase shifts between the consecutive images [3,10–12].

Recently, some significant attempts have been made on the DH with arbitrary coherence and with stochastic light such as optical scanning holography (OSH), Fresnel incoherent correlation holography (FINCH), and others [13–20]. OSH works on the principle of active optical heterodyne scanning. In OSH, a heterodyne interference fringe pattern is first generated without the information of the object, and the object target is then raster scanned via interference pattern [13]. In the FINCH, a hologram is composed of the summation of the Fresnel zone plate and recorded with incoherent light illumination using a single path and self-reference interferometer. An optical element [spatial light modulator (SLM), birefringent crystal, or double-focus lens] is introduced to generate two waves to record the incoherent hologram in the FINCH [15,16]. A polarization features of the light has been used in parallel phase-shifting incoherent holography and the hologram is recorded in a single shot with the polarization camera [17]. An imaging system with a low coherence illumination is also developed by combining microscopy with an off-axis holography geometry [18].

On the other hand, an unconventional holography technique named coherence holography (CH) is introduced to incoherently reconstruct the hologram and reconstruct the complex information as a distribution of the spatial coherence function [21]. The van Cittert–Zernike theorem and Hanbury Brown–Twiss (HBT) approach are two central results in the coherence optics and these two ideas are of paramount importance in the CH [21–23]. The CH employs an analogy between the optical field and coherence function to reconstruct a holographically recorded object from the two-point complex correlation of the random field. Incoherent light is used to illuminate the coherently recorded hologram and to synthesize the statistical features of the light for 3D imaging [21,23]. The CH has opened new research avenues on recording and shaping the spatial coherence for spatial coherence tomography, imaging, and coherence current, to name a few [24–27]. Designing an appropriate interferometer to measure spatial coherence is an extremely arduous task in the CH. Recording

*krakeshsingh.phy@iitbhu.ac.in

of incoherent object as a complex spatial coherence using the Sagnac interferometer with a phase-shifting approach has been developed [28]. In a recent development, the HBT approach was combined with off-axis holography to image the complex field in the correlation holography [29]. The relation between the second- and fourth-order Gaussian random field permits to use HBT approach in the CH and offers insight into statistical optics to develop simple and stable unconventional holography techniques [29–33]. Extension of the CH to the vectorial regime has also been demonstrated and some of these correlation holography techniques with polarization holograms are Stokes holography with second- and fourth-order interferometers [34,35]. These two vectorial holography techniques record information in the Stokes fringes and use incoherent illumination to reconstruct the polarimetric information. Recently, polarization fringes have also been used to develop phase-shifting coherence holography with the HBT approach [36] and in an enhanced field of view [37]. However, all these techniques demand an angular separation between interfering waves to implement phase recovery with the HBT approach. Such a situation requires resilient control over the reference field to record the interference fringes which limits the full utilization of the Fourier space and also affects the reconstruction quality.

In this paper, we propose a method for the reconstruction of the hologram with random light and demonstrate complex field recovery with the higher-order correlation. This technique exploits a fundamental feature of the light and uses higher-order Stokes parameters (SPs) correlation of the random light to build a reconstruction technique for the CH. This technique is free from the requirement of the angular separation between the interfering coherence waves and also offers a lensless Fourier transform connection between a desired two-point complex correlation at the observation plane with the incoherently illuminated hologram. Recently, SPs correlation was used to analyze random electromagnetic beams, ghost polarimetry, and to sense orbital angular momentum spectrum [38–41]. Inspired by the significance of the SPs in the characterization of the random fields, here we evolve a theoretical basis to develop a holographic principle for the reconstruction of the hologram with random light where conventional holography reconstruction methods fail. The SPs of the random light are used to extract SPs fluctuations correlations which imparts a 4×4 matrix with a total of 16 elements. Out of these 16 elements, only two elements of the matrix are utilized to develop a reconstruction method for the CH. The proposed theoretical basis with experimental results validates a reconstruction method for holography with random light. We attempt to build a holography technique without a carrier frequency in the fourth-order correlation, and the technique offers holographic reconstruction without phase shifting, and iteration, and is also free from a twin image issue. A detailed theoretical basis, simulation, and experimental results are discussed below.

II. BASIC PRINCIPLE

Consider a random orthogonally polarized light propagating along the z axis. The orthogonal polarization components of the light are expressed as

$$E_H(r) = |E_H(r)| \exp[i\varphi_H(r)], \;\; E_V(r) = |E_V(r)| \exp[i\varphi_V(r)]. \tag{1}$$

The subscripts H and V stand for horizontal and vertical polarization components and the coefficients $|E_H(r)|$ and $|E_V(r)|$ are the amplitude of the corresponding components with phases φ_H and φ_V, respectively. The light field can be represented as a column matrix:

$$E(r) = \begin{pmatrix} |E_H(r)| \exp[i\varphi_H(r)] \\ |E_V(r)| \exp[i\varphi_V(r)] \end{pmatrix}, \tag{2}$$

where $E(r)$ represents the field at a particular instant of time t. The polarimetric information of the field can be estimated as

$$S_p(r) = E^{\dagger}(r)\sigma^p E(r), \;\; (p = 0,\ 1,\ 2,\ 3), \tag{3}$$

where $\dagger$ denotes the Hermitian conjugate.σ^0 denotes the 2×2 identity matrix, and the three Pauli spin matrices are defined as

$$\sigma^1 = \begin{pmatrix} 1 & 0 \\ 0 & -1 \end{pmatrix}, \; \sigma^2 = \begin{pmatrix} 0 & 1 \\ 1 & 0 \end{pmatrix}, \; \sigma^3 = \begin{pmatrix} 0 & -i \\ i & 0 \end{pmatrix}. \tag{4}$$

A fluctuation of the Stokes parameter with respect to its mean value is evaluated as

$$\Delta S_p(r) = S_p(r) - \langle S_p(r) \rangle, \tag{5}$$

where $S_p(r)$ is the Stokes parameters at a particular spatial point and $\langle S_p(r) \rangle$ denotes the mean value. A correlation between two SPs fluctuations can be used to characterize the random light field. The 4×4 SPs fluctuation correlation matrix $C_{pq}(r_1, r_2)$ is defined as [38–40]

$$C_{pq}(r_1, r_2) = \langle \Delta S_p(r_1) \Delta S_q(r_2) \rangle, \;\; (p,\ q = 0,\ 1,\ 2,\ 3), \tag{6}$$

where r_1 and r_2 are two-position vectors at the observation plane and angle brackets $\langle . \rangle$ represent ensemble average. A fourth-order correlation can be expressed in terms of the second-order correlation for the Gaussian random fields. Therefore, elements of the matrix are expressed as [38,39]

$$C_{pq}(r_1, r_2) = \sum_{k,l} \sum_{m,n} \sigma^p_{kl} \sigma^q_{mn} W_{kn}(r_1, r_2) W^*_{lm}(r_1, r_2), \\ \times (k,\ l,\ m,\ n = x,\ y), \tag{7}$$

where $W_{kn}(r_1, r_2) = \langle E^*_k(r_1) E_n(r_2) \rangle$ represent elements of the 2×2 coherence-polarization (CP) matrix which characterize the statistical properties of the random field. The off-diagonal elements of the CP matrix are null for unpolarized light and represented as [39,42]

$$W(r_1, r_2) = \begin{pmatrix} W_{xx}(r_1, r_2) & 0 \\ 0 & W_{yy}(r_1, r_2) \end{pmatrix}. \tag{8}$$

Therefore, the 4×4 matrix is transformed to

$$C_{pq}(r_1, r_2) = \begin{pmatrix} |W_{xx}|^2 + |W_{yy}|^2 & |W_{xx}|^2 - |W_{yy}|^2 & 0 & 0 \\ |W_{xx}|^2 - |W_{yy}|^2 & |W_{xx}|^2 + |W_{yy}|^2 & 0 & 0 \\ 0 & 0 & 2\mathrm{Re}[W_{xx} W^*_{yy}] & 2\mathrm{Im}[W^*_{xx} W_{yy}] \\ 0 & 0 & 2\mathrm{Im}[W_{xx} W^*_{yy}] & 2\mathrm{Re}[W_{xx} W^*_{yy}] \end{pmatrix}. \tag{9}$$

For brevity, the (r_1, r_2) dependence of the matrix elements is suppressed on the left-hand side in Eq. (9). Two matrix elements $C_{22}(r_1, r_2)$, $C_{32}(r_1, r_2)$ are expressed as

$$C_{22}(r_1, r_2) = 2\mathrm{Re}[W_{xx}(r_1, r_2)W^*_{yy}(r_1, r_2)], \tag{10}$$

$$C_{32}(r_1, r_2) = 2\mathrm{Im}[W_{xx}(r_1, r_2)W^*_{yy}(r_1, r_2)]. \tag{11}$$

Here, we introduce a quantity called the complex polarization correlation function (CPCF) by adding Eqs. (10) and (11) as

$$C(r_1, r_2) = C_{22}(r_1, r_2) + iC_{32}(r_1, r_2), \tag{12}$$

$$C(r_1, r_2) \propto \mathrm{Re}[W_{xx}(r_1, r_2)W^*_{yy}(r_1, r_2)] + i\mathrm{Im}[W_{xx}(r_1, r_2)W^*_{yy}(r_1, r_2)] \tag{13}$$

where asterisk * denotes the complex conjugate.

Now, we examine use of Eq. (13) in the reconstruction of an incoherent object illuminated with random unpolarized light. Here, the object is an FTH encoding the complex-valued information as shown in Fig. 1(a) for application in the CH. This hologram is considered to be illuminated with an incoherent light in the reconstruction as shown in Fig. 1(b). The FTH can also be replaced by other real-valued objects as discussed in Refs. [28,43]. In order to use Eq. (13) in the CH and reconstruct the complex-valued object, a polarization component of the light illuminating the hologram is vertically polarized with desired coherence $W_{yy}(\Delta r)$. On the other hand, a horizontal polarization component is reserved for a reference coherence $W_{xx}(\Delta r)$.

The uniqueness of our strategy is also associated with independent control of two orthogonal polarization components, i.e., vertical for hologram illumination and horizontal for reference. A complex field represented in Eq. (2) is connected with the illuminating source as

$$E(r) = \int E(\hat{r}_1)h(r, \hat{r}_1)d\hat{r}_1, \tag{14}$$

$$E(r) = \frac{\exp(ikz)}{i\lambda z}\int \exp\left[\frac{ik}{2z}(|r|^2 - 2r.\hat{r}_1 + |\hat{r}_1|^2)\right]E(\hat{r}_1)d\hat{r}_1, \tag{15}$$

where $h(r, \hat{r}_j) = \frac{\exp(ikz)}{i\lambda z}\exp[\frac{ik}{2z}(r - \hat{r}_j)^2]$ is Fresnel kernel, λ wavelength of the incident beam, and $k = \frac{2\pi}{\lambda}$ represents wave number. A spatial position vector at the source plane is denoted by $\hat{r}_j$ $(j = 1, 2)$. Equation (14) represents an instantaneous complex field and a member of the ensemble. Substituting Eq. (14) into Eq. (12) helps to connect the CPCF with the elements of the CP matrix of the hologram and reference fields as follows:

$$C(r_1, r_2) = W^R_{xx}(r_1, r_2)W^{T^*}_{yy}(r_1, r_2) = \langle[E^{R^*}_x(r_1)E^R_x(r_2)]\rangle\langle[E^{T^*}_y(r_1)E^T_y(r_2)]^*\rangle, \tag{16}$$

where T and R stand for transmittance of a hologram or object and reference fields, respectively.

Substituting Eq. (15) into Eq. (16) transforms the complex coherence function as

$$W^T_{pp}(r_1, r_2) = \frac{1}{\lambda^2 z^2} < A\int\int E^*_p(\hat{r}_1)E_P(\hat{r}_2)\exp\left(\frac{ik}{2z}[|\hat{r}_2|^2 - |\hat{r}_1|^2]\right)\exp\left(\frac{-ik}{z}[r_2.\hat{r}_2 - r_1.\hat{r}_1]\right)d\hat{r}_1 d\hat{r}_2 >, \tag{17}$$

where p represents the orthogonal polarization component and T stands for transparency such as hologram or reference source. A phase term outside the integration is represented as $A = \exp(\frac{ik}{2z}|r_1|^2)\exp(-\frac{ik}{2z}|r_2|^2)$. A similar relation exists for a reference source illuminated by a horizontally polarized light. Substitution of the complex coherence functions for two orthogonal polarization components from Eq. (17) into Eq. (16) leads to the cancellation of a common phase curvature outside the integral and thus helps to achieve the spatial stationarity at an arbitrary z plane. Spatial stationarity at the observation plane permits replacing the ensemble averaging with a spatial averaging [42]. Ignoring phase terms outside the integration and considering $r_1 = r + \Delta r$ and $r_2 = r$, the use of spatial averaging at the observation plane transforms the complex coherence function as [42]

$$W^T_{pp}(r + \Delta r, r) = \int\int\left[\frac{1}{\lambda^2 z^2}\int \exp\left(\frac{ik}{2z}[|\hat{r}_2|^2 - |\hat{r}_1|^2]\right)\exp\left(\frac{-ik}{z}[(r + \Delta r).\hat{r}_2 - r.\hat{r}_1]\right)[E^*_p(\hat{r}_1)E_p(\hat{r}_2)]dr\right]d\hat{r}_1 d\hat{r}_2$$
$$= \frac{1}{\lambda^2 z^2}\int\int[E^*_p(\hat{r}_1)E_p(\hat{r}_2)]\delta(\hat{r}_2 - \hat{r}_1)\exp\left(\frac{-ik(\Delta r.\hat{r}_1)}{z}\right)d\hat{r}_1 d\hat{r}_2, \tag{18}$$

where $\int \exp(-\frac{ik}{z}(\hat{r}_2 - \hat{r}_1).r)dr = \delta(\hat{r}_2 - \hat{r}_1)$. Therefore, Eq. (18) transforms to

$$W^T_{pp}(\Delta r) \propto \int I^T_{pp}(\hat{r})\exp\left(-\frac{ik(\Delta r.\hat{r})}{z}\right)d\hat{r}, \tag{19}$$

where transmittance function for the hologram and reference are, respectively, $I_{yy}(\hat{r}) = |E_y(\hat{r})|^2$ and $I_{xx}(\hat{r}) = \mathrm{cir}(\frac{\hat{r}}{a})$, a represents aperture size at the scattering plane. The aperture size a is considered to be small in order to generate a uniform reference coherence $W^R_{xx}(\Delta r)$ to cover the support of $W^{T^*}_{yy}(\Delta r)$ as desired in Eq. (16). Therefore, Eq. (16) is represented as

$$W^R_{xx}(\Delta r)W^{T^*}_{yy}(\Delta r) \propto \int I_{yy}(\hat{r})\exp\left(\frac{ik(\Delta r.\hat{r})}{z}\right)d\hat{r}, \tag{20}$$

$I_{yy}(\hat{r})$ is a real function and represents the hologram. Equation (20) is a vectorial van Cittert–Zernike theorem based on spatial averaging and this relation connects an incoherently illuminated hologram with the complex coherence function at the z plane. Therefore, our strategy to independently deal with the orthogonal polarization components and to use random

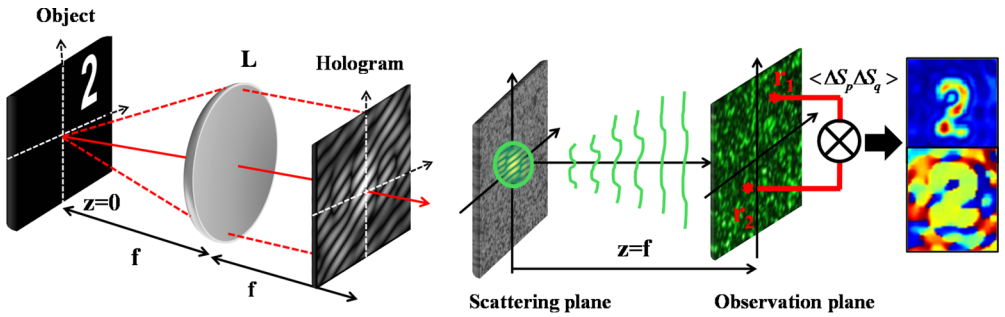

FIG. 1. Schematic representation of recoding and reconstruction of the FTH hologram. (a) Recording of the FTH hologram. L represents lens of focal length f. (b) Incoherent reconstruction of the FTH by random light at a distance $z = f$.

polarization in the higher-order Stokes parameters correlation helps to achieve a lensless Fourier transform with the coherence waves and hence reconstruct the FTH hologram by a single Fourier transform.

III. SIMULATION RESULTS

To illustrate validation of our approach, we simulate an experimental situation wherein a hologram is illuminated by the random field as represented in Fig. 1(b). An object located at an off-axis position as represented in Fig. 1(a) is encoded into the FTH. Conventional reconstruction of the FTH is not possible with random field illumination. We have simulated the Fourier hologram for two different objects, namely a vortex and a number 2 with $f = 250$ mm. A vortex is a phase object with a topological charge $l = 1$, where the topological charge represents a phase variation of 2π around the singularity [44]. Simulation is realized for orthogonally polarized random light fields with wavelength $\lambda = 532$ nm. The random fields for two orthogonal polarization components are modeled by considering two different and independent phase screens with phase variation with equal probability distribution in the range of $[-\pi, \pi]$. A random field coming out of the hologram is considered to be vertically polarized and propagation from the source to the observation plane at $z = 250$ mm is modeled using a Fresnel propagation kernel. Similarly, a horizontally polarized light emerging out of the reference phase screen propagates to the observation plane located at $z = 250$ mm using the Fresnel propagation kernel. A reference random field is generated by a circular aperture source of size $a = 0.8$ mm whereas the hologram size is 5 mm. Therefore, a random field at the observation plane comprises contributions from two independent and orthogonally polarized random sources, i.e., one from the hologram and the second from the reference. The Stokes parameters of the random field at the observation plane $z = 250$ mm are obtained from the digitally propagated coherent random fields. These simulated Stokes parameters are used to extract the higher-order Stokes fluctuations correlations as explained in Eq. (16) and utilized to reconstruct the hologram. The higher-order Stokes fluctuation correlations $C_{22}(\Delta r)$, $C_{32}(\Delta r)$ are obtained by using spatial averaging as follows.

Spatial averaging is implemented by taking a portion of the desired Stokes parameters of the speckle pattern at the observation plane as a matrix, $S_n^m(x, y)$ where $n = 2, 3$, and m represents a particular realization of the random field. Here, x and y are pixel spatial coordinates and take values up to 300 $\times$ 300 pixels. The Stokes fluctuation correlation is obtained by correlating $\Delta S_n^m(x, y)\Delta S_n^m(0, 0)$ for the deferent realization of the window of the speckle pattern and this process is represented as $\sum_{m=1}^{M} [\Delta S_n^m(x, y)\Delta S_n^m(0, 0)]/M$. Here, M represents the number of different realizations of the matrix $S_n^m(x, y)$ and which is produced by pixel by pixel movement of the matrix $S_n^m(x, y)$ over the speckle pattern. We have considered the window of size $(x, y) = 300 \times 300$ pixels and 2D scanning of $S_n^m(x, y)$ over the speckle pattern provides 700×700 different realizations in the spatial averaging. Out of the simulated SPs, only S_2 and S_3 are used to reconstruct the hologram as discussed in Eq. (12). The simulated reconstruction for two different holograms, namely with vortex and number 2, is shown in Fig. 2 using the Stokes fluctuation correlations. Figures 2(a) and 2(b) represent the amplitude distribution of the vortex and number 2 and Figs. 2(c) and 2(d) show corresponding phase distribution.

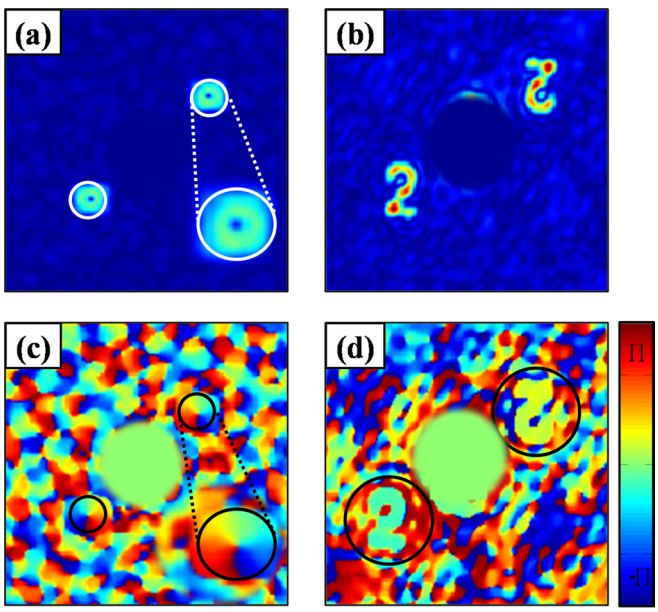

FIG. 2. Simulation results: (a), (b) Amplitude distribution of the vortex with $l = 1$ and number 2. (c), (d) Corresponding phase distribution. The magnified images of the amplitude and phase distribution of the vortex are shown in the inset of (a) and (c), respectively.

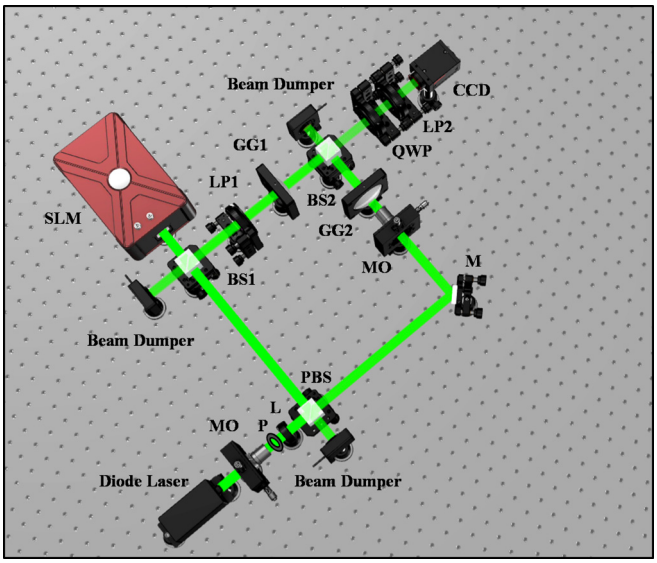

FIG. 3. Experimental implementation of the proposed technique. Laser: Solid random polarized diode laser, MO: Microscope objectives, P: Pinhole, L: lens, PBS: Polarizing beam splitter, M: Mirror, SLM: Spatial light modulator, GG1, GG2: Ground glasses, BS1, BS2: Beam splitters, QWP: Quarter-wave plate, LP1, LP2: Linear polarizers, CCD: Charge-coupled device.

IV. EXPERIMENT

Validation of the proposed technique is also confirmed by an experimental system designed in a collinear geometry as shown in Fig. 3. A spatially filtered collimated unpolarized diode laser light with a wavelength of 53-nm beam propagates through a polarization beam splitter (PBS) and subsequently, the beam divides into two orthogonal polarization components, i.e., horizontal and vertical. The PBS is used in the beginning to generate two independently orthogonally polarized random fields as follows. A vertical polarization component reflected by the PBS illuminates the spatial light modulator through a beam splitter (BS1). A beam reflected by the BS1, in the beginning, is dumped and not used in the experiment as represented by the beam dumper. A computer-generated hologram is displayed on the SLM (Holoeye LC-R 720) and loaded into reflected light from the SLM. This reflected beam is further guided by the BS1 towards a ground glass GG1and propagates towards the charge-coupled device (CCD). A linear polarizer (LP1) is placed after the BS1 to filter the vertical polarization component of the beam coming from the SLM. The distance between the hologram and the ground glass is considered to be negligible. The information encoded into the hologram is spatially scrambled by the diffuser GG1 and the speckle pattern of the vertically polarized light is produced at the observation plane without any direct resemblance to the object encoded into the FTH.

On the other hand, a transmitted horizontal polarization component from the PBS is folded by a mirror M and then focused by a microscope objective (MO-10×) at the ground-glass diffuser GG2 to generate a reference random field. The random field coming out of the GG2 is independent of the speckle of GG1 and this justifies consideration of no correlation of the orthogonal random fields at the observation plane, i.e., $< E_k^*(\hat{r}_1)E_l(\hat{r}_2) >= 0$. In order to measure the spatially varying SPs and characterize the random field at the observation plane, we inserted a quarter-wave plate (QWP) and linear polarizer (LP2) before the CCD. The SPs of the random light are measured by rotating the QWP at an angle θ_q to the x direction and filtering by an LP. The transmission axis of the LP is set in the x direction to the QWP and the resultant field is recorded by the CCD, which has a resolution of 2200×2750 pixels, a dynamic range of 8 bits, and a pixel pitch of $4.54\,\mu$m [Procilica, GT 2750]. The CCD is placed at a distance of $z = 250$ mm from the diffusers and this distance is the same as the focal length of digital lens f in the FTH as in Fig. 1(a). The two SPs are evaluated from the captured speckle pattern using the following equation [41]:

$$S_2(r) = I(45^\circ, 45^\circ) - I(135^\circ, 135^\circ), \tag{21}$$

$$S_3(r) = I(0^\circ, 45^\circ) - I(0^\circ, 135^\circ), \tag{22}$$

where $I(\theta_q, \theta_p)$ represent the intensity at the observation plane. θ_q, θ_p denote the orientation of the optic axis of QWP and LP with respect to the horizontal direction. The correlation between SP fluctuations is evaluated from the experimentally measured SPs as in Eq. (6) and using spatial averaging as a replacement for the ensemble averaging. This process provides the CPCF from the experimentally measured SPs as explained in Eq. (13). Finally, the recovered CPCF is used to reconstruct the complex amplitude encoded into the hologram.

V. EXPERIMENTAL RESULTS AND DISCUSSION

To experimentally test the proposed technique, we have taken two different holograms with a vortex and number 2 as explained in the simulation.

Experimentally measured desired SPs from the intensity speckle pattern for vortex and number 2 are shown in Fig. 4. The reconstructed amplitude and phase of the vortex with $l = 1$ from the random light are shown in Figs. 5(a) and 5(b). Likewise, the reconstructed amplitude and phase of the number 2 are shown in Figs. 5(c) and 5(d). The cross covariance of the experimentally recorded SPs (S_2, S_3) is evaluated by considering spatial averaging under the condition of spatial ergodicity at the observation plane (rather than in time). The mileages of the spatial averaging have been utilized recently in several correlation imaging approaches with due importance in spatial statistical optics [45]. The spatial averaging is implemented by using the following procedures. The experimentally recorded speckle pattern used in the evaluation process is of size 1000×1000 pixels. We have considered a window of size $(x, y) = 300 \times 300$ pixels for the display of spatial correlation and the remaining 700×700 for 2D scanning of $S_n^m(x, y)$ over the speckle pattern for different realizations and spatial averaging. In order to highlight the reconstruction of an off-axis hologram and highlight the reconstructed object, a central DC term is digitally suppressed as shown in Fig. 5.

The imaging quality of the proposed technique depends on the realization of the spatial stationarity of the random field at the CCD plane, the size of the polarization optics, and

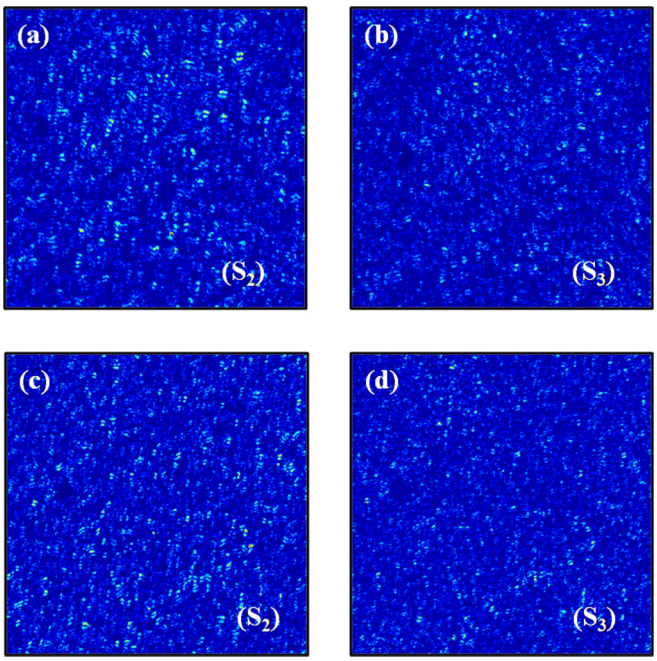

FIG. 4. Representation of experimentally measured SPs from the captured intensity patterns. (a), (b) SPs of the vortex with $l = 1$ (c), (d) SPs of number 2.

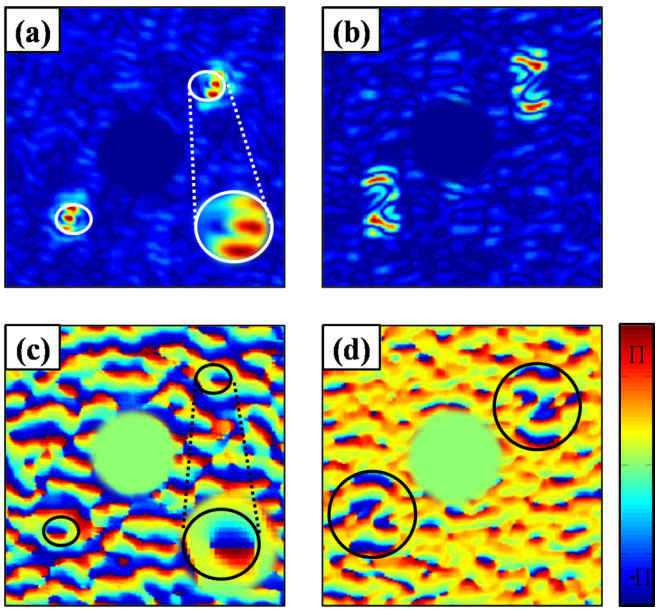

FIG. 5. Experimental results: (a), (b) Amplitude distribution of the vortex with $l = 1$ and number 2. (c), (d) Corresponding phase distribution. The magnified images of the amplitude and phase distribution of the vortex are shown in the inset of (a) and (c), respectively.

the incident source. The reconstruction quality is affected by the strength of the unpolarized source [46] and any leakage in the orthogonal polarization components due to optical elements will affect reconstruction quality. The reconstruction quality of the hologram is also affected owing to the short coherence length of the used random polarized diode laser in the experiment which brings coherent noise in the reconstructed phase [47].

VI. CONCLUSIONS

We have proposed and experimentally demonstrated a holography technique to reconstruct the complex amplitude of the object from stochastic light. The theoretical basis of the proposed technique is established and verified by simulation and experimental tests. The proposed experimental technique offers a reconstruction technique for holography with random light and its advantage lies in the ability to reconstruct complex fields without twin images and off-axis geometry. This work is expected to find applications in imaging through a random scattering medium, coherence analysis, and polarization-based imaging.

ACKNOWLEDGMENTS

We acknowledge support from the Science and Engineering Research Board (SERB) Grant No. CORE/2019/000026. The Department of Biotechnology (DBT) Grant No. BT/PR 35587/MED/32/707/2019 and the Council of Scientific and Industrial Research (CSIR) Grant No. 80 (0092)/20/EMR-II are acknowledged in this work. T.S. acknowledges the University Grant Commission, India for financial support as Senior Research Fellowship. V.T. acknowledges DST-INSPIRE (Grant No. IF-170861). S.C. acknowledges support from the IIT (BHU).

[1] D. Gabor, A new microscopic principle, Nature (London) **161**, 777 (1948).
[2] E. N. Leith and J. Upatnieks, Reconstructed wavefronts and communication theory, J. Opt. Soc. Am. **52**, 1123 (1962).
[3] I. Yamaguchi and T. Zhang, Phase-shifting digital holography, Opt. Lett. **22**, 1268 (1997).
[4] U. Schnars and W. Jüptner, *Digital Holography: Digital Hologram Recording, Numerical Reconstruction and Related Techniques* (Springer, Berlin, 2005).
[5] W. H. Lee, Sampled Fourier transform hologram generated by computer, Appl. Opt. **9**, 639 (1970).
[6] N. T. Shaked, Quantitative phase microscopy of biological samples using a portable interferometer, Opt. Lett. **37**, 2016 (2012).
[7] Y. Park, C. Depeursinge, and G. Popescu, Quantitative phase imaging in biomedicine, Nat. Photonics **12**, 578 (2018).
[8] V. Balasubramani *et al.*, Holographic tomography: Techniques and biomedical applications, Appl. Opt. **60**, B65 (2021).
[9] M. Gross, M. Atlan, and E. Absil, Noise and aliases in off-axis and phase-shifting holography, Appl. Opt. **47**, 1757 (2008).
[10] T. Nomura, B. Javidi, S. Murata, E. Nitanai, and T. Numata, Polarization imaging of a 3D object by use of on-axis phase-shifting digital holography, Opt. Lett. **32**, 481 (2007).
[11] Y. Awatsuji, A. Fujii, T. Kubota, and O. Matoba, Parallel three-step phase-shifting digital holography, Appl. Opt. **45**, 2995 (2006).

[12] V. Micó, J. García, Z. Zalevsky, and B. Javidi, Phase-shifting Gabor holography, Opt. Lett. **34**, 1492 (2009).

[13] J. P. Liu, T. Tahara, Y. Hayasaki, and T. C. Poon, Incoherent digital holography: A review, Appl. Sci. **8**, 143 (2018).

[14] G. Pedrini, H. Li, A. Faridian, and W. Osten, Digital holography of self-luminous objects by using a Mach–Zehnder setup, Opt. Lett. **37**, 713 (2012).

[15] J. Rosen and G. Brooker, Digital spatially incoherent Fresnel holography, Opt. Lett. **32**, 912 (2007).

[16] J. Rosen, A. Vijaykumar, M. Kumar, M. M. Rai, R. Kelner, Y. Kashter, A. Bulbul, and S. Mukherjee, Recent advances in self-interference incoherent digital holography, Adv. Opt. Photonics **11**, 1 (2019).

[17] T. Tahara, T. Kanno, Y. Arai, and T. Ozawa, Single-shot phase-shifting incoherent digital holography, J. Opt. **19**, 065705 (2017).

[18] P. Kolman and R. Chmelík, Coherence-controlled holographic microscope, Opt. Express **18**, 21990 (2010).

[19] Y. Cai and F. Wang, Lensless imaging with partially coherent light, Opt. Lett. **32**, 1359 (2007).

[20] N. Ohta, S. Kodama, Y. Miyamoto, W. Osten, M. Takeda, and E. Watanabe, 3D imaging through a highly heterogenous double-composite random medium by common-path phase-shift digital holography, Opt. Lett. **47**, 1170 (2022).

[21] M. Takeda, W. Wang, H. Z. Duan, and Y. Miyamoto, Coherence holography, Opt. Express **13**, 9629 (2005).

[22] J. Rosen, H. B. de Aguiar, V. Anand, Y. Baek, S. Gigan, R. Horisaki, H. Hugonnet, S. Juodkazis, K. Lee, H. Liang *et al.*, Roadmap on chaos-inspired imaging technologies (CI^2 – Tech), Appl. Phys. B **128**, 49 (2022).

[23] D. N. Naik, R. K. Singh, T. Ezawa, Y. Miyamoto, and M. Takeda, Photon correlation holography, Opt. Express **19**, 1408 (2011).

[24] Z. Duan, Y. Miyamoto, and M. Takeda, Dispersion-free optical coherence depth sensing with a spatial frequency comb generated by an angular spectrum modulator, Opt. Express **14**, 12109 (2006).

[25] W. Wang and M. Takeda, Coherence Current, Coherence Vortex, and the Conservation Law of Coherence, Phys. Rev. Lett. **96**, 223904 (2006).

[26] D. N. Naik, T. Ezawa, R. K. Singh, Y. Miyamoto, and M. Takeda, Coherence holography by achromatic 3-D field correlation of generic thermal light with an imaging Sagnac shearing interferometer, Opt. Express **20**, 19658 (2012).

[27] A. Dogariu and R. Carminati, Electromagnetic field correlations in three dimensional speckles, Phys. Rep. **559**, 1 (2015).

[28] D. N. Naik, G. Pedrini, and W. Osten, Recording of incoherent-object hologram as complex spatial coherence function using Sagnac radial shearing interferometer and a Pockels cell, Opt. Express **21**, 3990 (2013).

[29] R. K. Singh, R. V. Vinu, and A. M. Sharma, Recovery of complex valued objects from two-point intensity correlation measurement, Appl. Phys. Lett. **104**, 111108 (2014).

[30] N. K.Soni, R. Vinu, and R. K. Singh, Polarization modulation for imaging behind the scattering medium, Opt. Lett. **41**, 906 (2016).

[31] R. K. Singh, A. M. Sharma, and B. Das, Quantitative phase-contrast imaging through a scattering media, Opt. Lett. **39**, 5054 (2014).

[32] L. Chen, R. K. Singh, Z. Chen, and J. Pu, Phase shifting digital holography with the Hanbury Brown–Twiss approach, Opt. Lett. **45**, 212 (2020).

[33] R. V. Vinu, Z. Chen, R. K. Singh, and J. Pu, Ghost diffraction holographic microscopy, Optica **7**, 1697 (2020).

[34] R. K. Singh, D. N. Naik, H. Itou, Y. Miyamoto, and M. Takeda, Stokes holography, Opt. Lett. **37**, 966 (2012).

[35] D. Singh and R. K. Singh, Lensless Stokes holography with the Hanbury Brown-Twiss approach, Opt. Express **26**, 10801 (2018).

[36] L. Chen, R. K. Singh, R. V. Vinu, Z. Chen, and J. Pu, A wavefront division multiplexing holographic scheme and its application in looking through diffuser, New. J. Phys. **23**, 113034 (2021).

[37] L. Chen, Z. Chen, R. K. Singh, R. V. Vinu, and J. Pu, Increasing field of view and signal to noise ratio in the quantitative phase imaging with phase shifting holography based on the Hanbury Brown-Twiss approach, Opt. Lasers Eng. **148**, 106771 (2022).

[38] G. Wu, D. Kubel, and T. D. Visser, Generalized Hanbury Brown-Twiss effect in partially coherent electromagnetic beams, Phys. Rev. A **99**, 033846 (2019).

[39] D. Kuebel and T. D. Visser, Generalized Hanbury Brown-Twiss effect for stokes parameters, J. Opt. Soc. Am. A **36**, 362 (2019).

[40] A. Hannonen, B. J. Hoenders, W. Elsässer, A. T. Friberg, and T. Setälä, Ghost polarimetry using Stokes correlations, J. Opt. Soc. Am. A **37**, 714 (2020).

[41] T. Sarkar, R. Parvin, M. M. Brundavanam, and R. K. Singh, Higher-order Stokes parameters correlation to restore twisted wavefront propagating through a scattering medium, Phys. Rev. A **104**, 013525 (2021).

[42] R. K. Singh, D. N. Naik, H. Itou, M. M. Burndavanam, Y. Miyamoto, and M. Takeda, Vectorial van Cittert-Zernike theorem based on spatial averaging: Experimental demonstrations, Opt. Lett. **38**, 4809 (2013).

[43] R. K. Singh, S. Vyas, and Y. Miyamoto, Lensless Fourier transform holography for coherence waves, J. Opt. **19**, 115705 (2017).

[44] J. P. Torres and L. Torner, *Twisted Photons, Application of Light with Orbital Angular Momentum* (Wiley-VCH, Weinheim, Germany, 2011).

[45] M. Takeda, W. Wang, D. N. Naik, and R. K. Singh, Spatial statistical optics and spatial correlation holography: A review, Opt. Rev. **21**, 849 (2014).

[46] H. Kellock, T. Setälä, T. Shirai, and A. T. Friberg, Image quality in double- and triple-intensity ghost imaging with classical partial polarized light, J. Opt. Soc. Am. A **29**, 2459 (2012).

[47] Y. L. Lee, Y. C. Lin, H. Y. Tu, and C. J. Cheng, Phase measurement accuracy in digital holographic microscopy using a wavelength-stabilized laser diode, J. Opt. **15**, 025403 (2013).